

Receive Beamforming Designed for Massive Multi-User MIMO Detection via Gaussian Belief Propagation

Takanobu DOI^{†a)}, Jun SHIKIDA[†], Daichi SHIRASE[†], *Members*, Kazushi MURAOKA[†], *Senior Member*, Naoto ISHII[†], Takumi TAKAHASHI^{††}, *Members*, and Shinsuke IBI^{†††}, *Senior Member*

SUMMARY This paper proposes two full-digital receive beamforming (BF) methods for low-complexity and high-accuracy uplink signal detection via Gaussian belief propagation (GaBP) at base stations (BSs) adopting massive multi-input multi-output (MIMO) for open radio access network (O-RAN). In addition, beyond fifth generation mobile communication (beyond 5G) systems will increase uplink capacity. In the scenarios such as O-RAN and beyond 5G, it is vital to reduce the cost of the BSs by limiting the bandwidth of fronthaul (FH) links, and the dimensionality reduction of the received signal based on the receive BF at a radio unit is a well-known strategy to reduce the amount of data transported via the FH links. In this paper, we clarify appropriate criteria for designing a BF weight considering the subsequent GaBP signal detection with the proposed methods: singular-value-decomposition-based BF and QR-decomposition-based BF with the aid of discrete-Fourier-transformation-based spreading. Both methods achieve the dimensionality reduction without compromising the desired signal power by taking advantage of a null space of channels. The proposed receive BF methods reduce correlations between the received signals in the BF domain, which improves the robustness of GaBP against spatial correlation among fading coefficients. Simulation results assuming realistic BS and user equipment arrangement show that the proposed methods improve detection capability while significantly reducing the computational cost.

key words: massive MIMO, receive beamforming, O-RAN, belief propagation, deep unfolding

1. Introduction

Beyond fifth generation mobile communication (beyond 5G) systems are expected to be a platform to realize cyber physical systems (CPSs). In CPSs, uplink wireless communications will play a vital role to upload massive sensing data from a physical world to a cyber world, leading to explosive increase in uplink traffic. To increase the capacity of the uplink communications, massive multi-user multi-input multi-output (MU-MIMO) techniques [1], which spatially multiplex transmitted signals from multiple users, have been investigated. The number of multiplexing signals is expected to increase to meet the uplink capacity demand in beyond 5G era.

In the MU-MIMO, multi-user detection (MUD) is processed to detect transmitted signals from multiple users in the base stations (BSs). As typical low complexity MUDs, linear spatial filterings, such as matched filter (MF), zero forcing (ZF) filter, and minimum mean square error (MMSE) filter, are low-accurate methods in terms of bit error rate (BER) performance. In contrast, maximum likelihood (ML) detection is the optimal MUD, but its computational cost is prohibitively high. In order to achieve a reasonable complexity-accuracy trade-off, belief propagation (BP) algorithms have been proposed, such as Gaussian BP (GaBP) [2], approximate message passing (AMP) [3], generalized approximate message passing (GAMP) [4], and expectation propagation (EP) [5]. These BP algorithms provide iterative MUD schemes which gradually improve detection accuracy by exchanging beliefs, i.e., likelihood information reflecting detection reliability, across iterations. Considering the potential of the BP algorithms in massive MIMO assumed in beyond 5G systems, this paper adopts low-complexity MUD based on GaBP.

Another trend of mobile communication systems gaining attention is an open radio access network (O-RAN) [6]–[8]. The O-RAN enables the flexible configuration of BSs. In O-RAN-compliant BSs, the physical layer functions are split into the low physical layer in a radio unit (RU) and the high physical layer in a distributed unit (DU), which are connected via fronthaul (FH) links [9]. While the RU performs analog and/or digital beamforming (BF), the DU performs baseband signal processing, such as MUD, mapping/demapping, and channel coding/decoding. The standardization of the FH interface, for example enhanced common public radio interface (eCPRI) [10], enables mobile network operators to flexibly combine the RUs and the DUs from different vendors to build BSs satisfying various wireless communication service requirements.

As a significant part of the cost of an O-RAN-compliant BS is the optical devices in the FH links, using narrower bandwidth FH should contribute to reducing the cost of the BS. In the uplink, the required bandwidth of the FH links depends on the amount of data traffic transported from the RU to the DU. When adopting the massive MU-MIMO techniques [1] to improve the end-to-end uplink capacity, a significant increase in the capacity of the FH links is inevitable to transport the high-dimensional received signals. One promising approach to solve this issue is full-digital receive BF at the RU, which reduces the dimension of the re-

Manuscript received October 7, 2022.

Manuscript revised January 24, 2023.

Manuscript publicized March 8, 2023.

[†]The authors are with NEC Corporation, Kawasaki-shi, 211-8666 Japan.

^{††}The author is with Osaka University, Suita-shi, 565-0871 Japan.

^{†††}The author is with Doshisha University, Kyotanabe-shi, 610-0394 Japan.

a) E-mail: doi-takanobu@nec.com

DOI: 10.1587/transcom.2022FGP0004

ceived signals from the number of receive antenna elements equipped on the RU to the number of spatial multiplexed transmitted streams. Note that one of disadvantages of the full-digital receive BF is high hardware complexity, because the RU requires as many analog-to-digital converters (ADCs) and digital-to-analog converters (DACs) as receive antenna elements.

In [11] and [12], the receive BF, which is constructed on the basis of QR decomposition of channel matrices, is applied to iterative signal detectors based on BP. These methods enable to improve the detection performance by reducing the number of short loops on the factor graph, which represents the MUD problem using a linear transformation by the BF methods. However, the classical BP [11] requires marginalization operations based on the factor graph structure, resulting in high computational burden. To reduce the computational cost, GaBP in [2] takes advantage of the Gaussian approximation (GA) of residual interference signals based on the central limit theorem in parallel interference cancellation (PIC). However, when an effective channel matrix after the receive BF is not suitable for GA in the subsequent GaBP-based signal detection, the performance severely deteriorates. This is true for an upper triangular effective channel matrix obtained by the receive BF based on QR decomposition. To address this issue, the authors of [12] modified the message-passing rule of GaBP to use successive interference cancellation (SIC) instead of PIC to effectively deal with the upper triangular channel matrix. However, the SIC algorithm generally takes longer processing time than PIC due to successive processing [13]. From a practical point of view, the original GaBP with PIC is still desirable in terms of short processing time and low computational complexity.

In light of the above, our aim is to design an appropriate full-digital receive BF so that the original PIC-based GaBP operates properly. To the best of our knowledge, this study is the first to combine the PIC-based GaBP with receive BF. First, we present the following three criteria for the full-digital receive BF weights: (i) maintain the whiteness of the noise, (ii) maintain the desired signal power, and (iii) improve the GA accuracy of residual interference signals. While the first two criteria are the primary criteria for the subsequent stochastic signal processing to work well, the third criterion is specialized for PIC-based GaBP. In addition, it is desirable to design a receive BF which can suppresses spatial correlation among fading coefficients, because the spatial correlation severely degrades the detection accuracy of GaBP.

In this paper, we propose two receive BF construction methods to satisfy the three criteria: singular value decomposition-based BF (SVD-BF) and QR decomposition-based BF with the aid of discrete Fourier transformation (DFT) matrix-based spreading (QR-DFT-BF). SVD-BF can greatly improve detection capability by making the beamformed received signals uncorrelated with each other. QR-DFT-BF with lower computational cost can also improve detection capability while suppressing the correlation. To overcome the vulnerability of GaBP to the spatial correla-

tion, we instead use trainable GaBP (T-GaBP) [14], the internal parameters embedded in the iterative process of which are trained using deep learning techniques; this technique is referred to as deep unfolding [15]. By training T-GaBP, including the proposed receive BF methods, we can optimize the structure of T-GaBP to be fully consistent with the proposed BF methods. It is also worth noting here that the dimensionality reduction contributes to reducing the computational cost of GaBP. Finally, simulation results demonstrate the efficacy of the proposed methods with the receive BF in terms of the detection capability and the computational cost.

This paper is an extension of [16], including a more detailed description of the algorithm and more realistic scenarios in the computer simulations. More specifically, an arrangement of a BS and user equipment (UE) devices is more realistic than the arrangement in [16]. The BS is set at higher position than UEs in this paper, while the BS and UEs were set at the same height in [16]. The number of spatially multiplexed streams is increased to 24 considering the beyond 5G system. In addition, low-density parity check (LDPC) code [17] is used as a forward error correction (FEC) code, whereas no FEC code is assumed in [16]. The rest of this paper is organized as follows. In Sect. 2, we show configurations of the system and signal model. Section 3 describes the detailed algorithm of multi-user detection via GaBP and T-GaBP, respectively. In Sect. 4, we propose two receive BF methods suitable for GaBP and T-GaBP. Section 5 provides numerical results about the detection accuracy of T-GaBP with the proposed receive BF. Finally, in Sect. 6, we conclude this paper.

2. System Model

2.1 Configuration of Base Station and System

Consider an uplink massive MU-MIMO system composed of a BS and several synchronized UE devices. The BS has N receive antennas in a uniform planar array pattern. Each UE device has M_T transmit antennas, and the number of UE devices is M_{UE} , i.e., the total number of transmit antennas is $M = M_T \times M_{UE}$, where M is less than N . The number of multiplexing signals is usually much smaller than that of antenna elements mounted on the receiver at a BS to reduce the number of reference signals from UE devices. Thus, M transmit signals are spatially multiplexed. Note that transmit BF is not applied in each UE for simplicity of analysis.

Figure 1 shows an example of a block diagram of the BS that consists of an RU and a DU in consideration of the O-RAN specifications. The RU executes digitization of receive signals, cyclic prefix (CP) removal, fast Fourier transformation (FFT), and receive digital BF, whereas the DU executes channel estimation, BF weight generation, and MUD. Signals are transported using orthogonal frequency division multiplexing (OFDM) and are transformed from the time domain to the frequency domain in the RU. The UE devices transmit sounding reference signals (SRS), which are received at the RU. The received SRS without receive BF

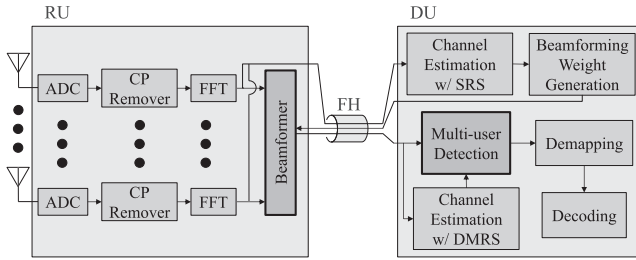


Fig. 1 BS processing consisting of RU and DU for uplink.

are transported from the RU to DU. Using the SRS, the DU estimates channels between every UE device and the RU then generates receive BF weights using the knowledge of the estimated channels. The generated weights are transported to the RU and set at the beamformer. The UE devices transmit data signals with demodulation reference signals (DMRS) to the RU. The RU executes receive beamforming for both the received data signals and DMRS, which can reduce the dimension of the received signals from the number of receive antenna elements to the number of spatially multiplexed streams, then the reduced beamformed received signals are transported to the DU. The DU executes channel estimation using the DMRS, which results in an estimation of the beamformed effective channel matrix. The DU executes MUD using signal detectors such as T-GaBP with the beamformed received signals and the estimated channel matrix. Finally, the DU demaps the detected signals to log-likelihood ratio (LLR) and decodes the LLR to data bit sequence. The SRS, BF weights, DMRS, and data signals are transported between the RU and the DU via the FH.

2.2 Signal Model

Throughout this paper, following notations are used. Vectors and matrices are denoted by lower- and upper-case bold-face letter, respectively. \cdot^T and \cdot^H are the transpose and Hermitian transpose operator, respectively. \mathbf{I}_a is an $a \times a$ identity matrix and $\mathbf{O}_{a \times b}$ is an $a \times b$ zero matrix. $\|\cdot\|$ represents a L2 norm of a vector. Furthermore, $(\cdot)_i$ and $(\cdot)_{i,j}$ are the i -th vector element and the i -th row and the j -th column matrix element, respectively. \mathbb{R} and \mathbb{C} are denote real and complex fields, respectively. $\Re\{\cdot\}$ and $\Im\{\cdot\}$ denote the real and imaginary parts of a complex value, respectively. $CN(a, b)$ indicates a complex-valued Gaussian process with a mean a and a variance b . $\mathbb{E}_a\{\cdot\}$ is the expected value of random variable a .

In this paper, OFDM is assumed as the transmission scheme. Nevertheless, we omit the subcarrier index of variables because we focus on one of the subcarriers hereafter. We use quadrature amplitude modulation (QAM) whose modulation order is Q , with the m -th transmit antenna conveying a modulated symbol x_m . A transmitted signal vector $\mathbf{x} \in \mathbb{C}^{M \times 1}$ and received signal vector $\mathbf{y} \in \mathbb{C}^{N \times 1}$ of a subcarrier are represented as

$$\mathbf{x} = [x_1 \ \dots \ x_m \ \dots \ x_M]^T, \quad (1)$$

$$\mathbf{y} = [y_1 \ \dots \ y_n \ \dots \ y_N]^T = \mathbf{H}\mathbf{x} + \mathbf{z}, \quad (2)$$

where $\mathbf{H} \in \mathbb{C}^{N \times M}$ and $\mathbf{z} \in \mathbb{C}^{N \times 1}$ are a MIMO channel matrix and a noise vector of the subcarrier, respectively. The noise vector $\mathbf{z} = [z_1 \ \dots \ z_n \ \dots \ z_N]^T$ is a complex additive white Gaussian noise vector with entries z_n obeying $CN(0, N_0)$, where $\mathbb{E}_{\mathbf{z}}\{\mathbf{z}\mathbf{z}^H\} = N_0\mathbf{I}_N$ and N_0 is noise power density. At the RU, the receive BF is applied to Eq. (2). The beamformed effective received signal vector $\mathbf{y}' \in \mathbb{C}^{M \times 1}$ is given by

$$\mathbf{y}' = \mathbf{W}^H \mathbf{y} = \mathbf{H}'\mathbf{x} + \mathbf{z}', \quad (3)$$

where $\mathbf{W}^H \in \mathbb{C}^{M \times N}$ is a receive BF weight. The beamformed effective channel matrix and the beamformed noise vector are respectively represented as

$$\mathbf{H}' = \mathbf{W}^H \mathbf{H} \in \mathbb{C}^{M \times M}, \quad (4)$$

$$\mathbf{z}' = \mathbf{W}^H \mathbf{z} \in \mathbb{C}^{M \times 1}, \quad (5)$$

As shown in Eq. (3), the receive BF reduces the dimension of the received signals from N to M , which can reduce the required bandwidth of the FH links.

3. Multi-User Detection via Trainable Gaussian Belief Propagation

This paper adopts T-GaBP for a MUD method, which iteratively estimates a transmitted signal using GaBP with the internal parameters trained by deep unfolding [15]. The structure of T-GaBP encompasses techniques for BP-based iterative detection to improve the convergence property, i.e., belief damping [18], node selection [19], and belief scaling [20]. GaBP and T-GaBP are respectively explained in the following subsections.

3.1 Gaussian Belief Propagation (GaBP)

GaBP is one of MF based BP algorithms. Figure 2 shows a block diagram of GaBP that consists of three modules: soft interference canceller (Soft IC), belief generator (BG), and soft replica generator (Soft RG). Table 1 presents the pseudo-code of the GaBP, where $\cdot^{(k)}$ for each variable indicates the corresponding variable at the k -th iteration. Alg- s indicates the s -th step in Table 1. For ease of algebraic manipulations, the complex-valued signal model of Eq. (3) can be converted to a double-size real valued signal model on the basis of pulse amplitude modulation (PAM) symbols as follows:

$$\mathbf{y}^{r'} = \mathbf{H}^{r'} \mathbf{x}^r + \mathbf{z}^{r'}, \quad (6)$$

$$\mathbf{y}^{r'} = \begin{bmatrix} \Re\{\mathbf{y}'\} \\ \Im\{\mathbf{y}'\} \end{bmatrix} = \begin{bmatrix} y_1^r \\ \vdots \\ y_m^r \\ \vdots \\ y_{2M}^r \end{bmatrix} \in \mathbb{R}^{2M \times 1}, \quad (7)$$

$$\mathbf{H}^{r'} = \begin{bmatrix} \Re\{\mathbf{H}'\} & -\Im\{\mathbf{H}'\} \\ \Im\{\mathbf{H}'\} & \Re\{\mathbf{H}'\} \end{bmatrix}$$

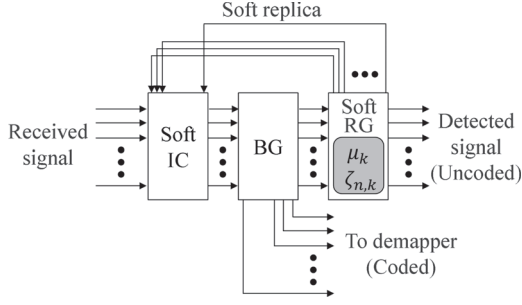


Fig. 2 Block diagram of GaBP.

Table 1 Pseudo-code of Gaussian belief propagation.

Input:	$\mathbf{y}^r, \mathbf{H}^r, K, C = \{\zeta_{n,k}, \mu_k, \forall n, k\}$
Output:	$\hat{\mathbf{x}} = [\hat{x}_1, \dots, \hat{x}_m, \dots, \hat{x}_{2M}]^T$
	// Initialization
1:	$\mathcal{N} = \{1, \dots, 2N\}, \mathcal{M} = \{1, \dots, 2M\}$
2:	$\mathcal{G}_Q = \{2l \cdot c l = 0, \pm 1, \dots, \pm (\frac{\sqrt{Q}}{2} - 1)\}$
3:	$\forall n, m: \tilde{x}_{n,m}^{(0)} = 0, \tilde{e}_{n,m}^{(0)}, \theta_{n,m} = h_{n,m}^r$
4:	$\forall n, m: u_{n,m}^{(0)} = 0, v_{n,m}^{(0)} = 0$
5:	for $k = 1$ to K do
	// Soft interference canceller (Soft IC)
6:	$\forall n, m: \tilde{y}_{n,m}^{(k)} = y_n^r - \sum_{i \neq m} h_{n,i}^r \tilde{x}_{n,i}^{(k-1)}$
7:	$\forall n, m: \delta_{n,m}^{(k)} = \tilde{e}_{n,m}^{(k-1)} - (\tilde{x}_{n,m}^{(k-1)})^2$
	// Belief generator (BG)
8:	$\forall n, m: \psi^{(k)}(k)_{n,m} = \sum_{i \neq m} \theta_{n,i} \delta_{n,i}^{(k)} + \frac{N_0}{2}$
9:	$\forall n, m: u_{n,m}^{(k)} = \frac{h_{n,m}^r \tilde{y}_{n,m}^{(k)}}{\psi_{n,m}^{(k)}}, v_{n,m}^{(k)} = \frac{\theta_{n,m}}{\psi_{n,m}^{(k)}}$
10:	$\forall n, m: u_{n,m}^{(k)} = \zeta_{n,k} \cdot u_{n,m}^{(k)} + (1 - \zeta_{n,k}) \cdot u_{n,m}^{(k-1)}$
11:	$\forall n, m: v_{n,m}^{(k)} = \zeta_{n,k} \cdot v_{n,m}^{(k)} + (1 - \zeta_{n,k}) \cdot v_{n,m}^{(k-1)}$
12:	$\forall n, m: s_{n,m}^{(k)} = \sum_{i \neq n} u_{i,m}^{(k)}, \omega_{n,m}^{(k)} = \sum_{i \neq n} v_{i,m}^{(k)}$
13:	$\forall n, m: \gamma_{n,m}^{(k)} = \frac{s_{n,m}^{(k)}}{\omega_{n,m}^{(k)}}$
	// Soft replica generator (Soft RG)
14:	$\forall n, m: \tilde{x}_{n,m}^{(k)} = c \sum_{\gamma' \in \mathcal{G}_Q} \tanh \left[\frac{\mu_k}{c} \cdot (\gamma_{n,m}^{(k)} - \gamma') \right]$
15:	$\forall n, m: \tilde{e}_{n,m}^{(k)} = (\sqrt{Q} - 1)^2 c^2$ $+ 2c \sum_{\gamma' \in \mathcal{G}_Q} \gamma' \cdot \tanh \left[\frac{\mu_k}{c} \cdot (\gamma_{n,m}^{(k)} - \gamma') \right]$
16:	end for k

$$= \begin{bmatrix} h_{1,1}^r & \cdots & h_{1,2M}^r \\ \vdots & h_{n,m}^r & \vdots \\ h_{2M,1}^r & \cdots & h_{2M,2M}^r \end{bmatrix} \in \mathbb{R}^{2M \times 2M}, \quad (8)$$

$$\mathbf{x}^r = \begin{bmatrix} \Re\{\mathbf{x}\} \\ \Im\{\mathbf{x}\} \end{bmatrix} = \begin{bmatrix} x_1^r \\ \vdots \\ x_m^r \\ \vdots \\ x_{2M}^r \end{bmatrix} \in \mathbb{R}^{2M \times 1}, \quad (9)$$

$$\mathbf{z}^r = \begin{bmatrix} \Re\{\mathbf{z}'\} \\ \Im\{\mathbf{z}'\} \end{bmatrix} = \begin{bmatrix} z_1^r \\ \vdots \\ z_m^r \\ \vdots \\ z_{2M}^r \end{bmatrix} \in \mathbb{R}^{2M \times 1}, \quad (10)$$

where the m -th PAM symbol x_m^r in \mathbf{x}^r represents one of the $Q' (= \sqrt{Q})$ PAM constellation points in $X = \{\pm(2i - 1)c | i = 1, 2, \dots, Q'/2\}$ [21]. Let us define a coefficient $c = \sqrt{3E_s/2(Q-1)}$ for normalizing the average power density of X to $E_s/2$. For example, we have $X = \{\pm c, \pm 3c\}$ and $c = \sqrt{E_s/10}$, when 16QAM ($Q = 16$) is used.

Soft IC subtracts the inter-user interference from each received signal by using the soft replicas generated in the previous iteration as shown in Alg-6. Note that the soft replicas are initialized by 0 at the first iteration step. BG generates the beliefs as described in Alg-8–Alg-12 by approximating the residual interference-plus-noise in the output of Soft IC as independent and identically distributed (i.i.d.) Gaussian noise following the central limit theorem. This behavior is referred to as scalar Gaussian approximation (SGA). After computing the beliefs under SGA, Soft RG approximately calculates the conditional expectation of the transmitted symbol in Alg-14 and Alg-15. GaBP processes these modules iteratively. When the number of iterations reaches the pre-determined value K , BG outputs beliefs to demapper in Fig. 1 to generate the LLR. Although GaBP shows excellent performance under spatially uncorrelated MIMO channels, the spatial correlation among fading coefficients occurring in real environment degrades the performance.

To improve the accuracy of detection, belief damping, node selection and belief scaling are applied to GaBP. Belief damping [18] gives the current belief by a weighted average of the belief at the current iteration step and the belief obtained in the previous iteration step. Node selection [19] determines a subset of beliefs to be updated at each iteration on the basis of the BS antenna pattern to improve the robustness against correlated MIMO channels. This node selection is generalized by introducing a weighting parameter, $\zeta_{n,k}$, for the n -th antenna and the k -th iteration, where $0 \leq \zeta_{n,k} \leq 1$. The weighting include character of both the belief damping and the node selection. This weighting parameter at each iteration enables the dynamic change in the subset, which can reduce correlation among beliefs and accelerate convergence speed. Belief scaling [20] adjusts the reliability of beliefs at each iteration to prevent degradation caused by low-precision beliefs. Parameter μ_k is a scaling parameter at the k -th iteration for belief scaling.

3.2 Trainable GaBP (T-GaBP)

Figure 3 shows the structure of T-GaBP which unfolds the iterative structure of GaBP and optimizes the parameters with data-driven training technique of deep learning [22]. T-GaBP trains the internal parameters of GaBP, such as $\zeta_{n,k}$ and μ_k . One iteration of GaBP corresponds to one layer of deep neural network. Training data consists of many pairs of received signals and transmitted signals. In the training phase of T-GaBP, a mean-square-error (MSE) loss function L is calculated by the following equation:

$$L = \frac{1}{D} \sum_{d=1}^D \|\mathbf{x}^r[d] - \hat{\mathbf{x}}^{(K)}[d]\|^2, \quad (11)$$

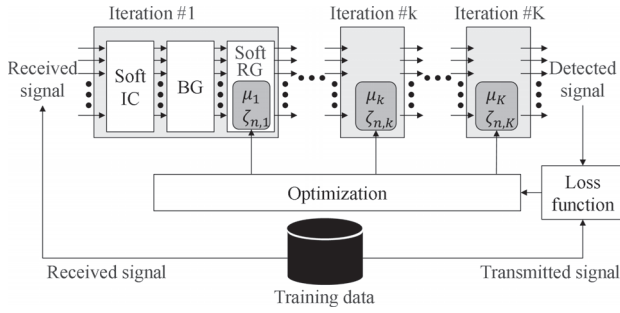


Fig. 3 Structure of T-GaBP.

where D is the number of training data, $\mathbf{x}^r[d] \in \mathbb{R}^{2M \times 1}$ is the transmitted signal of the d -th training data, and $\tilde{\mathbf{x}}^{(K)}[d] \in \mathbb{R}^{2M \times 1}$ is the soft replica vector generated at the K -th iteration for the d -th training data. The parameters $\zeta_{n,k}$ and μ_k are optimized to minimize the loss L . After training the parameters of T-GaBP, MUD is processed with GaBP in Fig. 2 whose parameters are set to trained parameters. It would be realistic for the trainable parameters to be learned in advance by computer simulations in several different settings and then tabulated and incorporated at the time of BS installation. In this case, the learned parameters must be robust to various radio environments that vary depending on the BS location and surrounding situations. Therefore, we recognize that the learning method to obtain such robust parameters is vital for future work. However, in the deep unfolding technology [15] used in this study, the most part of the algorithm is constructed using a model-based design approach that can take environmental information, e.g., instantaneous CSI, into account, and the number of learning parameters is much smaller than that of conventional learning models. Based on the above, we believe that even at present the proposed algorithm has some robustness to changes in the statistical properties of the data handled, and in fact, we have obtained some data showing such initial results. In this study, these parameters were trained using beamformed received signals to optimize the parameters for MUD with receive BF.

4. Receive Beamforming

Since the analytical derivation of the optimal receive BF weight for GaBP is difficult, we design the receive BF weight considering the feature of GaBP. The following three criteria are considered for the design of the receive BF weight \mathbf{W}^H .

- (i) Receive BF maintains the whiteness of the noise without enhancing the intensity of noise.
- (ii) Receive BF does not lose the desired signal power.
- (iii) Receive BF converts the receive signals so that inter-user interference in the beam domain can be approximated as Gaussian distribution with high accuracy.

Criteria (i) and (ii) are aimed at maintaining signal-detection accuracy after receive BF. Criterion (iii) is specialized for the subsequent GaBP.

Criterion (i) is satisfied when a \mathbf{W}^H consists of M or-

thonormal vectors. If the following equation:

$$\mathbf{W}^H \mathbf{W} = \mathbf{I}_M, \quad (12)$$

holds, the beamformed noise can maintain the whiteness as

$$\mathbb{E}_{\mathbf{z}} \{ \mathbf{z}' \mathbf{z}'^H \} = N_0 \mathbf{I}_M. \quad (13)$$

Criterion (ii) requires that the desired signal power before receive BF, i.e., $\text{tr}(\mathbf{H}^H \mathbf{H})$, is equal to that after receive BF, i.e., $\text{tr}(\mathbf{H}'^H \mathbf{H}')$, represented as

$$\text{tr}(\mathbf{H}^H \mathbf{H}) = \text{tr}(\mathbf{H}'^H \mathbf{H}'). \quad (14)$$

Criterion (iii) is approximately satisfied when elements of the beamformed effective channel matrix $\mathbf{W}^H \mathbf{H}$ are unbiased, which is explained in more detail later.

4.1 Receive Beamforming Using Singular Value Decomposition (SVD-BF)

We developed SVD-BF as a receive BF method satisfying criteria (i), (ii), and (iii), which uses a partial left singular matrix, i.e., the BF weight matrix is given by

$$\mathbf{W}^H = \mathbf{U}_0^H, \quad (15)$$

where $\mathbf{U}_0^H \in \mathbb{C}^{M \times N}$ is the partial left singular matrix, which is derived from SVD as

$$\mathbf{H} = [\mathbf{U}_0 \quad \mathbf{U}_1] \begin{bmatrix} \mathbf{\Gamma} \\ \mathbf{O}_{(N-M) \times N} \end{bmatrix} \mathbf{V}^H, \quad (16)$$

where $[\mathbf{U}_0 \quad \mathbf{U}_1] \in \mathbb{C}^{N \times N}$ is a left singular matrix, $\mathbf{\Gamma} \in \mathbb{R}^{M \times M}$ is a singular value matrix which is a diagonal matrix, and $\mathbf{V} \in \mathbb{C}^{M \times M}$ is a right singular matrix. The i -th diagonal element of $\mathbf{\Gamma}$ is $\gamma_i \in \mathbb{R}$. The beamformed effective channel matrix of SVD-BF is given by

$$\mathbf{H}' = \mathbf{\Gamma} \mathbf{V}^H. \quad (17)$$

Since \mathbf{U}_0 is a submatrix of a unitary matrix, \mathbf{U}_0 satisfies criterion (i) as

$$\mathbf{U}_0^H \mathbf{U}_0 = \mathbf{I}_M. \quad (18)$$

From Eq. (18), we can obtain the following relationship:

$$\begin{aligned} \mathbf{H}^H \mathbf{H} &= (\mathbf{U}_0 \mathbf{\Gamma} \mathbf{V}^H)^H \mathbf{U}_0 \mathbf{\Gamma} \mathbf{V}^H \\ &= (\mathbf{\Gamma} \mathbf{V}^H)^H \mathbf{U}_0^H \mathbf{U}_0 \mathbf{\Gamma} \mathbf{V}^H \\ &= (\mathbf{\Gamma} \mathbf{V}^H)^H \mathbf{\Gamma} \mathbf{V}^H = \mathbf{H}'^H \mathbf{H}'. \end{aligned} \quad (19)$$

Thus, criterion (ii) is satisfied as

$$\text{tr}(\mathbf{H}^H \mathbf{H}) = \text{tr}(\mathbf{H}'^H \mathbf{H}'). \quad (20)$$

SVD-BF can be interpreted as the utilization of a part of a unitary-transformed channel $[\mathbf{U}_0 \quad \mathbf{U}_1]^H \mathbf{H}$. The space of the channel reduced by SVD-BF corresponds to

$$\mathbf{U}_1^H \mathbf{H} = \mathbf{O}_{(N-M) \times N}. \quad (21)$$

This means no power is included in the reduced space $\mathbf{U}_1^H \mathbf{H}$, and all the power of the channel is concentrated in $\mathbf{U}_0^H \mathbf{H}$. Therefore, using SVD-BF enables dimensionality reduction without compromising the desired signal power by taking advantage of a null space of the channels. Moreover, criterion (iii) is satisfied because the elements of the effective channel matrix of Eq. (17) are generated via spreading using the unitary matrix.

As shown in Eq. (19), a transmitting Gram matrix of the beamformed effective channel matrix $\mathbf{H}'^H \mathbf{H}'$ does not change from a transmitting Gram matrix of the original channel matrix $\mathbf{H}^H \mathbf{H}$. On the other hand, a receiving Gram matrix after receive BF changes to a diagonal matrix as follows:

$$\begin{aligned} \mathbf{H}'^H \mathbf{H}' &= \mathbf{\Gamma} \mathbf{V}^H (\mathbf{\Gamma} \mathbf{V}^H)^H \\ &= \mathbf{\Gamma}^2 = \begin{bmatrix} \gamma_1^2 & 0 & \dots & 0 \\ 0 & \gamma_2^2 & \dots & 0 \\ \vdots & \vdots & \ddots & \vdots \\ 0 & 0 & \dots & \gamma_M^2 \end{bmatrix}. \end{aligned} \quad (22)$$

The off-diagonal elements contribute to correlations between different beamformed signals. From Eq. (22), we can say that different beamformed signals are uncorrelated for SVD-BF. This stochastic property helps improving the performance of GaBP and T-GaBP by reducing correlations between beliefs.

4.2 Receive Beamforming Using QR Decomposition and DFT Matrix (QR-DFT-BF)

The receive BF introduced by the authors of [11] and [12] uses the submatrix of the unitary matrix created by QR decomposition of the channel matrix as

$$\mathbf{W}^H = \mathbf{Q}_0^H, \quad (23)$$

$$\mathbf{H} = \begin{bmatrix} \mathbf{Q}_0 & \mathbf{Q}_1 \end{bmatrix} \begin{bmatrix} \mathbf{R} \\ \mathbf{O}_{(N-M) \times M} \end{bmatrix}, \quad (24)$$

where $[\mathbf{Q}_0 \ \mathbf{Q}_1] \in \mathbb{C}^{N \times N}$ is a unitary matrix, and $\mathbf{R} \in \mathbb{C}^{M \times M}$ is an upper triangular matrix. We refer to Eq. (23) as QR-BF. The beamformed effective channel matrix of QR-BF is given by

$$\mathbf{H}' = \mathbf{R}. \quad (25)$$

Since $\mathbf{Q}_0 \in \mathbb{C}^{N \times M}$ is a submatrix of a unitary matrix, \mathbf{Q}_0 satisfies criterion (i) as

$$\mathbf{Q}_0^H \mathbf{Q}_0 = \mathbf{I}_M. \quad (26)$$

From Eq. (24), we can confirm that criterion (ii) is satisfied as

$$\begin{aligned} \text{tr}(\mathbf{H}^H \mathbf{H}) &= \text{tr}(\mathbf{R}^H \mathbf{Q}_0^H \mathbf{Q}_0 \mathbf{R}) \\ &= \text{tr}(\mathbf{R}^H \mathbf{R}) = \text{tr}(\mathbf{H}'^H \mathbf{H}'). \end{aligned} \quad (27)$$

However, criterion (iii) is not satisfied for QR-BF because the effective channel matrix of QR-BF is an upper triangular

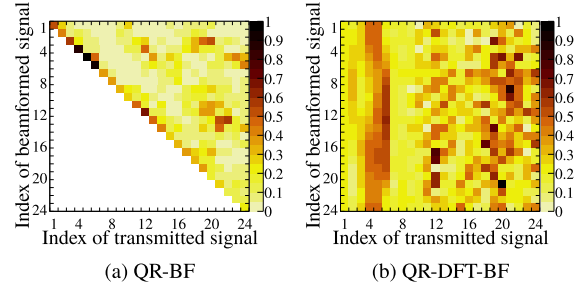


Fig. 4 Examples of effective channel matrix.

Table 2 Number of real multiplications of each processing.

Method		Number of real multiplication
BF	SVD-BF	$\frac{32}{3} T M^3 + 8 N M^2$
	QR-DFT-BF	$(20T + 6) M^2 - (\frac{92T}{3} + 2) M$
MUD	T-GaBP without BF	$4((\sqrt{Q} + 18) K - \sqrt{Q} - 3) N M + 6 M$
	T-GaBP with BF	$4((\sqrt{Q} + 18) K - \sqrt{Q} - 3) M^2 + 6 M$
	MMSE	$4 M^3 + 8 N M^2 + 4 N M$

matrix, i.e., highly biased. Figure 4(a) shows an example of the effective channel matrix of QR-BF, which is generated using the clustered delay line (CDL) A model [23], where the intensity of each element is depicted. This highly biased structure severely degrades the SGA accuracy of inter-user interference, resulting in ill-convergence behavior of GaBP iterative detection.

To reduce the bias of the effective channel matrix, we introduce spreading operations using the DFT matrix \mathbf{W}_{DFT} to QR-BF as

$$\mathbf{W}^H = \mathbf{W}_{\text{DFT}}^H \mathbf{Q}_0^H, \quad (28)$$

which is referred to as QR-DFT-BF. The effective channel matrix for QR-DFT-BF is given by

$$\mathbf{H}' = \mathbf{W}_{\text{DFT}} \mathbf{R}, \quad (29)$$

where the DFT matrix disperses non-zero elements over the effective channel matrix of Eq. (29), as shown in Fig. 4(b), to satisfy criterion (iii). Since the DFT matrix is a unitary matrix, criteria (i) and (ii) are also satisfied. It is worth mentioning that the spreading matrix does not necessarily have to be a DFT matrix; thus, another unitary matrix can be used in Eq. (28) as an alternative.

4.3 Comparison of Complexity to Generate BF Weight

Table 2 shows the number of real multiplications required for SVD-BF, QR-DFT-BF, T-GaBP, and MMSE. The Jacobi method is used for calculating SVD, whereas Gram-Schmidt orthonormalization is used for QR decomposition. The T is the number of iterations of the Jacobi method for SVD, and is about 10 when $M = 24$. The dominant terms in each method are the first and the second terms ($\frac{32}{3} T M^3 + 8 N M^2$) in SVD-BF, the first term ($6 N M^2$) in QR-DFT-BF, the first

and the second terms $(4(\sqrt{Q} + 18)KNM)$ in T-GaBP without BF, the first and the second terms $(4(\sqrt{Q} + 18)KM^2)$ in T-GaBP with BF, and the first and second terms $(4M^3 + 8NM^2)$ in MMSE. For example, let us assume M , N , and T are 24, 64, and 10, respectively. In this case QR-DFT-BF requires about 1/7 of multiplications than SVD-BF does, because QR decomposition requires fewer real multiplications than SVD.

5. Numerical Results

Computer simulations were conducted to validate the performance of the T-GaBP with the proposed receive BF methods. Table 3 lists the simulation conditions. The transmission scheme is OFDM, where each subcarrier is modulated by Gray-coded 16QAM. LDPC [17] code, whose code rate is about 2/3, is used as a FEC code. The center frequency, bandwidth, and subcarrier spacing are set to 4 GHz, 100 MHz and 30 kHz, respectively. The number of subcarrier is 3276 that consists of 273 resource blocks and 12 subcarriers per resource block. For the channel model, the CDL-A model [23], which is a non-line-of-sight (NLOS) model, is used with 100-ns delay spread.

Figure 5 shows the configuration of a BS and UE devices. The BS and UE devices have cross polarization antennas. The BS has a uniform planar array pattern antenna with four rows and eight columns, where each element has a pair of polarization antennas. Thus, the total number at the BS antennas is 64. The antenna spacing is set to a half wavelength. The BS antenna is set at 10 m high position from UE's height that is 1.5 m. The UE devices have a pair of polarization antennas. We assume 12 UE devices, so the total number of UE antennas is 24. The total number of multiplexing is 24, where the number of the spatial multiplexing and that of the polarization-division multiplexing are 12 and 2, respectively. The 12 UE devices are arranged in a rectangle pattern which has three rows and four columns with 20-m interval. The center of UEs is 50 m away from the BS. Although the distances between each UE and the BS are different, we assume the average signal-to-noise power ratios (SNRs) at the BS of different UE devices are the same in uplink communication. This assumption is true when the differences in the path loss due to the different distances from the BS to each UE are compensated by uplink transmission power control. Both the channel estimation using SRS and that using DMRS are assumed to be ideal. Thus, perfect channel knowledge is assumed on the BS side. Trainable parameters in T-GaBP are optimized for each of the proposed methods, the number of transmit and receive antenna elements, and the number iterations of T-GaBP respectively. The SNR of the training data is 15 dB. The initial values of the trainable parameters of T-GaBP are set as follows:

$$\mu_k = 2 \cdot \frac{k}{K}, \quad (30)$$

$$\zeta_{n,k} = \begin{cases} \text{sigmoid}(2) & \text{if } k - n \equiv 0 \pmod{4} \\ \text{sigmoid}(-2) & \text{otherwise} \end{cases}, \quad (31)$$

Table 3 Simulation conditions.

Item	Value
Transmission scheme	OFDM
Center frequency	4 GHz
Bandwidth	100 MHz
Subcarrier spacing	30 kHz
Number of subcarriers	3276 (= 273 × 12)
Modulation scheme	Gray-coded 16QAM
Forward error correction	LDPC [17]
Coding rate	2/3
Number of antennas at the BS	64
Number of antennas mounted on one UE	2
Number of UEs	12
Number of multiplexing	24
Speed of user equipment	Static
Channel model	CDL-A (NLOS) [23]
Channel estimation	Ideal
Optimizer of T-GaBP	Adam [24]
SNR of training data	15 dB

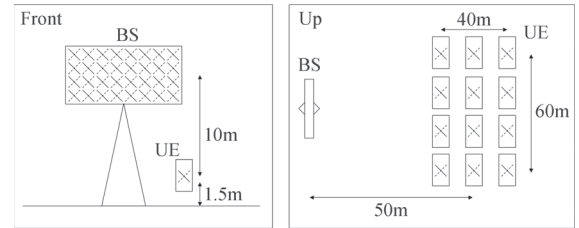


Fig. 5 Configuration of BS and UE devices.

where n , k , and K are the index of the received signal, the index of the iteration, and the number of iterations, respectively.

5.1 BER Performance

Figure 6 shows the BER performance of different detectors in $(N, M) = (64, 24)$ MIMO systems, where the number of iterations of T-GaBP is 40. For comparison, curves of a MMSE filter and T-GaBP without receive BF are also drawn. MMSE is a typical linear filter and is considered a baseline performance. The performance of T-GaBP without BF has a high-level error floor at $\text{BER} > 10^{-2}$ because of the strong spatial correlation among receive antenna elements. In contrast, T-GaBP with QR-DFT-BF has a lower error floor and exhibits better performance than MMSE when $\text{SNR} \leq 16$ dB. However, due to the error floor around BER of 10^{-3} , T-GaBP with QR-DFT-BF is worse than MMSE in the high SNR region. When $\text{SNR} > 12$ dB, T-GaBP with SVD-BF achieves the best performance where an error floor does not appear, at least above BER of 10^{-5} . The gain of T-GaBP with SVD-BF from MMSE at BER of 10^{-3} is about 4 dB. To confirm the necessity of criterion (iii), we also evaluated T-GaBP with QR-BF. As expected, a high error floor above BER of 10^{-1} is shown for T-GaBP with QR-BF because QR-BF does not satisfy criterion (iii).

The reason for the improvement of BER performance in T-GaBP with the receive BF is that it reduces correlations

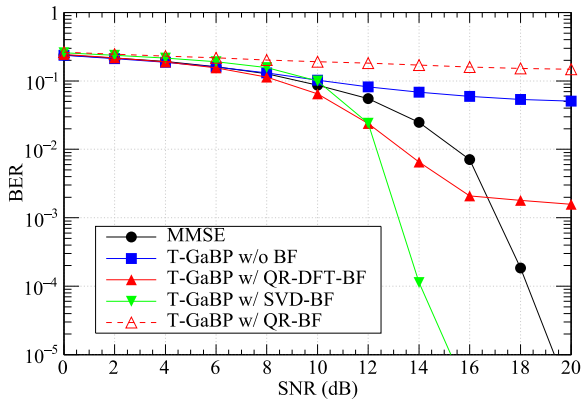


Fig. 6 Bit error rate performance of T-GaBP with BF, T-GaBP without BF, and MMSE.

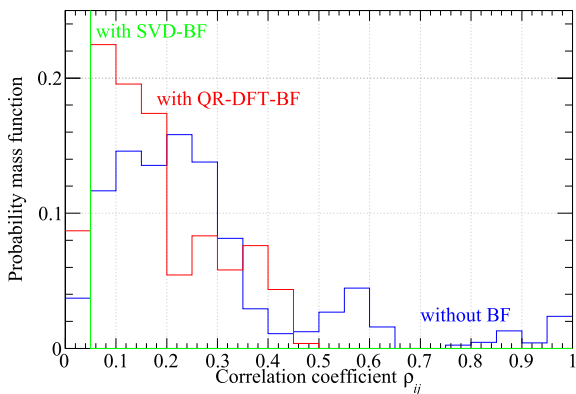


Fig. 7 Probability mass function of correlations between received signals.

between beamformed signals compared with those between received signals before the receive BF. Figure 7 illustrates the probability mass function of the correlation between two received signals at high SNR, where the correlation coefficient between the i -th beamformed signal and j -th beamformed signal is calculated as

$$\begin{aligned} \rho_{ij} &= \frac{\mathbb{E}_{\mathbf{y}'} \left\{ y'_i y'^*_{j'} \right\}}{\sqrt{\mathbb{E}_{\mathbf{y}'} \left\{ |y'_i|^2 \right\} \mathbb{E}_{\mathbf{y}'} \left\{ |y'_{j'}|^2 \right\}}} \\ &\approx \frac{\mathbb{E}_{\mathbf{H}'} \left\{ \left(\mathbf{H}' \mathbf{H}'^H \right)_{i,j} \right\}}{\sqrt{\mathbb{E}_{\mathbf{H}'} \left\{ \left(\mathbf{H}' \mathbf{H}'^H \right)_{i,i} \right\} \mathbb{E}_{\mathbf{H}'} \left\{ \left(\mathbf{H}' \mathbf{H}'^H \right)_{j,j} \right\}}}. \quad (32) \end{aligned}$$

$(N_0 \ll |(\mathbf{H}' \mathbf{x})_i|^2, \forall i)$

Remarkably, some pairs of received signals before receive BF are highly correlated with the correlation coefficient of about 0.95. By contrast, the correlations after receive BF are reduced to smaller than 0.5. More specifically, the received signals beamformed using SVD-BF are uncorrelated, as shown in Eq. (22). Some pairs are correlated after QR-DFT-BF with a larger value than SVD-BF, but they are

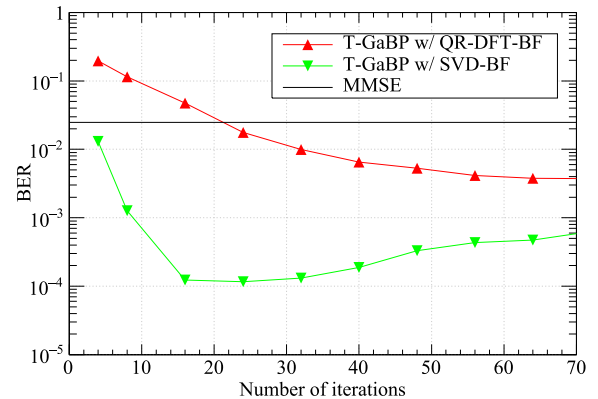


Fig. 8 BER v.s. the number of iterations in $(N, M) = (64, 24)$ MIMO at SNR = 14 dB.

greatly reduced compared with the correlation, as in the case without receive BF.

Figure 8 shows the BER versus the number of iterations of T-GaBP with SVD-BF and QR-DFT-BF at SNR of 14 dB. The BER performance of both the BF methods improves as the number of iterations increases. However, each method has different convergence properties. The BER of T-GaBP with QR-DFT-BF converges when the number of iterations is 64. The BER of T-GaBP with SVD-BF rapidly decreases and reaches the bottom with 24 iterations. The reason that T-GaBP with SVD-BF has rapid decrease of BER is due to the no correlation of the beamformed received signals, which makes it possible to generate high-precision beliefs at early iterations. On the other hand, BER of T-GaBP with SVD-BF gets worse when the number of iterations increases from 24. This is because the parameters of T-GaBP with SVD-BF having a large number of iterations are not sufficiently trained. As it corresponds to a deep neural network with many layers, vanishing gradients in the neural network make the training difficult. However, this problem was not observed in T-GaBP with QR-DFT-BF. This difference comes from the fact that the precision of beliefs of T-GaBP with SVD-BF is higher than that of T-GaBP with QR-DFT-BF because of lower BERs. In other words, signal replicas generated at Soft RG in T-GaBP with SVD-BF are almost hard decisions, which result in risk causing vanishing gradients. This training of the parameters of T-GaBP with SVD-BF for a large number of iterations becomes our future work.

5.2 Comparison of Computational Complexity of MUD

Figure 9 shows the number of real multiplications for MUD with receive BF in accordance with the number of receive antennas. M , Q , and T are set to 24, 16, and 10, respectively. K is set to 24 in T-GaBP with SVD-BF and is set to 64 in T-GaBP with QR-DFT-BF based on Fig. 8. K in T-GaBP without BF is assumed to be the same number of iterations in T-GaBP with QR-DFT-BF, because T-GaBP without BF cannot improve detection capability no matter how much the number of iterations is increased. Therefore, no argument for its convergence can be made. MMSE has the lowest

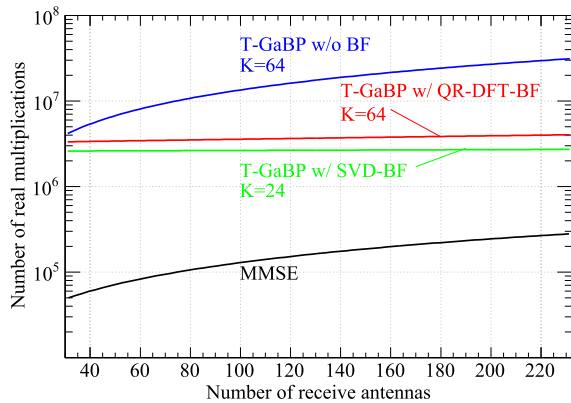


Fig. 9 Number of real multiplications in $M = 24$.

complexity, which is less than 1/10 of the complexity of T-GaBP ($K=24$) with SVD-BF, although signal detection performance of MMSE is worse than T-GaBP with SVD-BF, as shown in Fig. 6. The number of real multiplications of T-GaBP without BF increases as the number of received antennas increases. However, the increase in the complexity of T-GaBP with BF is small even if the number of receive antennas increases. The complexity of T-GaBP is much larger than those of SVD-BF and QR-DFT-BF when the number of iterations K is large. When the receive BF is not applied, the complexity of T-GaBP depends on the number of dimensions of receive antennas. In contrast, when the receive BF is applied, the complexity of T-GaBP depends on the number of dimensions of the beamformed signal that is equal to the number of transmit antennas, and does not depend on the number of receive antennas. As a result, the increase in the complexity of T-GaBP with BF is small even if the number of receive antennas increases. Regarding calculation of the BF weight, SVD-BF requires more real multiplications than QR-DFT-BF does. However, the total number of real multiplications of T-GaBP ($K=24$) with SVD-BF is almost the same as that of T-GaBP ($K=64$) with QR-DFT-BF, since T-GaBP with SVD-BF requires fewer iterations than T-GaBP with QR-DFT-BF as illustrated in Fig. 8.

6. Conclusion

We proposed two receive BF methods (SVD-BF and QR-DFT-BF) for improving T-GaBP-based detection capability for massive MU-MIMO. These BF methods were designed considering three criteria suitable for GaBP and can reduce correlations between two received signals. Numerical results indicate that T-GaBP with the proposed methods is superior to both MMSE and T-GaBP without receive BF because of the reduced correlations. In particular, T-GaBP with SVD-BF shows large improvements in the high SNR region, where an error floor does not appear owing to uncorrelated beamformed signals. In addition, generating the SVD-BF requires more real multiplications than generating the QR-DFT-BF does; however, since the T-GaBP with SVD-BF can converge to the solution within fewer iterations than T-

GaBP with QR-DFT-BF, and therefore the total number of real multiplications of T-GaBP with SVD-BF is almost the same as that of T-GaBP with QR-DFT-BF. These methods pave the way to reducing FH bandwidth and cost reductions for BSs.

References

- [1] E. Telatar, "Capacity of multi-antenna Gaussian channels," *Eur. Trans. Telecommun.*, vol.10, no.6, pp.585–595, 1999. DOI: 10.1002/ett.4460100604
- [2] Y. Kabashima, "A CDMA multiuser detection algorithm on the basis of belief propagation," *J. Phys. A: Math. Gen.*, vol.36, no.43, pp.11111–11121, 2003. DOI: 10.1088/0305-4470/36/43/030
- [3] D.L. Donoho, A. Maleki, and A. Montanari, "Message passing algorithms for compressed sensing: I. motivation and construction," 2010 IEEE Information Theory Workshop on Information Theory (ITW 2010, Cairo), pp.1–5, 2010. DOI: 10.1109/ITWIKSPS.2010.5503193
- [4] S. Rangan, "Generalized approximate message passing for estimation with random linear mixing," 2011 IEEE International Symposium on Information Theory Proceedings, pp.2168–2172, 2011. DOI: 10.1109/ISIT.2011.6033942
- [5] J. Cespedes, P.M. Olmos, M. Sanchez-Fernandez, and F. Perez-Cruz, "Expectation propagation detection for high-order high-dimensional MIMO systems," *IEEE Trans. Commun.*, vol.62, no.8, pp.2840–2849, 2014. DOI: 10.1109/TCOMM.2014.2332349
- [6] O-RAN ALLIANCE, "O-RAN working group 1; O-RAN architecture description v04.00," <https://orandownloadweb.azurewebsites.net/specifications>, accessed Oct. 7, 2022.
- [7] W. Diego, "Evolution toward the next generation radio access network," 2020 IFIP Networking Conference (Networking), June 2020.
- [8] S.K. Singh, R. Singh, and B. Kumbhani, "The evolution of radio access network towards open-RAN: Challenges and opportunities," 2020 IEEE Wireless Communications and Networking Conference Workshops (WCNCW), April 2020.
- [9] J. Gomes, J.A.L. Silva, and M.E.V. Segatto, "Reducing the 5G fronthaul traffic with O-RAN," 2019 SBMO/IEEE MTT-S International Microwave and Optoelectronics Conference (IMOC), pp.1–3, 2019. DOI: 10.1109/IMOC43827.2019.9317620
- [10] CPRI Common Public Radio Interface, "Common public radio interface: Requirements for the eCPRI transport network, v1.2 ed.," <http://www.cpri.info/spec.html>, accessed Oct. 7, 2022.
- [11] S. Park and S. Choi, "QR decomposition aided belief propagation detector for MIMO systems," *Electron. Lett.*, vol.51, no.11, pp.873–874, 2015. DOI: 10.1049/el.2015.0378
- [12] S. Tanabe, A.D. Shigyo, and K. Ishibashi, "Not-so-large MIMO signal detection based on damped QR-decomposed belief propagation," 2016 International Symposium on Information Theory and Its Applications (ISITA), pp.463–467, 2016.
- [13] T. Manglayev, R.C. Kizilirmak, and Y.H. Kho, "Comparison of parallel and successive interference cancellation for non-orthogonal multiple access," 2018 International Conference on Computing and Network Communications (CoCoNet), pp.74–77, 2018. DOI: 10.1109/CoCoNet.2018.8476815
- [14] D. Shirase, T. Takahashi, S. Ibi, K. Muraoka, N. Ishii, and S. Sampei, "Deep unfolding-aided Gaussian belief propagation for correlated large MIMO detection," *IEEE Global Communications Conference (GLOBECOM)*, pp.1–6, 2020. DOI: 10.1109/GLOBECOM42002.2020.9348087
- [15] J.R. Hershey, J.L. Roux, and F. Wenginger, "Deep unfolding: Model-based inspiration of novel deep architectures," *arXiv: 1409.2574*, 2014.
- [16] T. Doi, J. Shikida, K. Muraoka, N. Ishii, D. Shirase, T. Takahashi, and S. Ibi, "Receive beamforming for Gaussian belief propagation in massive multi-user MIMO for reducing fronthaul bandwidth," 2022 IEEE Wireless Communications and Networking Conference (WCNC),

- pp.1359–1364, 2022. DOI: 10.1109/WCNC51071.2022.9771674
- [17] D.J. MacKay, “Good error-correcting codes based on very sparse matrices,” *IEEE Trans. Inf. Theory*, vol.45, no.2, pp.399–431, 1999. DOI: 10.1109/18.748992
- [18] P. Som, T. Datta, A. Chockalingam, and B.S. Rajan, “Improved large-MIMO detection based on damped belief propagation,” 2010 IEEE Information Theory Workshop on Information Theory (ITW 2010, Cairo), pp.1–5, 2010. DOI: 10.1109/ITWKSPPS.2010.5503188
- [19] M. Hagiwara, T. Nishimura, T. Ohgane, and Y. Ogawa, “Node selection and LLR damping for channel equalization with belief propagation,” 2016 International Symposium on Information Theory and Its Applications (ISITA), pp.483–487, 2016.
- [20] T. Takahashi, S. Ibi, and S. Sampei, “Design of adaptively scaled belief in multi-dimensional signal detection for higher-order modulation,” *IEEE Trans. Commun.*, vol.67, no.3, pp.1986–2001, 2019. DOI: 10.1109/TCOMM.2018.2883307
- [21] J. Lu, K.B. Letaief, J. C-I. Chuang, and M.L. Liou, “M-PSK and M-QAM BER computation using signal-space concepts,” *IEEE Trans. Commun.*, vol.47, no.2, pp.181–184, 1999. DOI: 10.1109/26.752121
- [22] Y. Lecun, L. Bottou, Y. Bengio, and P. Haffner, “Gradient-based learning applied to document recognition,” *Proc. IEEE*, vol.86, no.11, pp.2278–2324, 1998. DOI: 10.1109/5.726791
- [23] 3GPP, “Technical specification group radio access network study on channel model for frequencies from 0.5 to 100 GHz,” <https://www.3gpp.org/DynaReport/38901.htm>, accessed Oct. 7, 2022.
- [24] D.P. Kingma and J. Ba, “Adam: A method for stochastic optimization,” arXiv: 1412.6980, 2017.



Kazushi Muraoka received the B.S. degree in computer science, the M.S. degree, and the Ph.D. degree in communications and integrated systems, all from Tokyo Institute of Technology, Tokyo, Japan, in 2005, 2007, and 2013, respectively. He joined NEC Corporation in 2007, where he was engaged in research on cellular networks, cognitive radios, and wireless sensor networks. In 2014, he was a visiting researcher at University of California, Berkeley. From 2018 to 2019, he was engaged in research on 5G mobile communication systems in NTT DOCOMO, INC. He is currently involved in research on 6G mobile communication systems in NEC Corporation. His research interests include radio signal processing and radio resource management. He received the Young Researchers' Award from IEICE in 2012.



Naoto Ishii received his B.E. degree, M.E. degree and Ph.D. degree in electrical engineering from Yokohama National University in 1992, 1994 and 1997, respectively. He joined NEC Corporation, Japan in 1997. He is currently working for the research of 6G mobile communication. His research interests include signal processing and radio resource management for mobile wireless communication systems. He received the Young Researchers' Award from IEICE in 1998.



Takanobu Doi received the B.S. and M.S. degrees in science from Kyoto University in 2018 and 2020, respectively. Since joining NEC Corporation in 2020, he engaged in multi-user detection, signal processing, and wireless communication. He received the Young Researchers' Award from IEICE in 2021.



Takumi Takahashi received his B.E., M.E., and Ph.D. degrees in communication engineering from Osaka University, Osaka, Japan, in 2016, 2017, and 2019, respectively. From 2018 to 2019, he was a visiting researcher at the Centre for Wireless Communications, University of Oulu, Finland. In 2019, he joined the Graduate School of Engineering, Osaka University as an assistant professor. His research interests include belief propagation, compressed sensing, signal processing, and wireless communications.



Jun Shikida received the B.E. and M.E. degrees in electrical and electronic engineering from Tokyo Institute of Technology, Tokyo, Japan, in 2009 and 2011, respectively. He joined NEC Corporation in 2011. His research interests include signal processing and wireless communication. He received the Young Researchers' Award from IEICE in 2018.



Shinsuke Ibi received the B.E. degree in advanced engineering from Suzuka College of Technology, Japan, in 2002, and the M.E. and Ph.D. degrees in communication engineering from Osaka University, Japan, in 2004 and 2006, respectively. From 2005 to 2006, he was a visiting researcher at the Centre for Wireless Communications, University of Oulu, Finland. In 2006, he joined the Graduate School of Engineering, Osaka University. From 2010 to 2011, he was a visiting researcher at the University of Southampton, United Kingdom. In 2019, he moved to Doshisha University, and he is currently a professor in the Faculty of Science and Engineering. His research interests include EXIT-based coding theory, iterative detection, digital signal processing, cognitive radio, and communication theory. He received the 64th and 71st Best Paper Awards from IEICE, 2017, 2018, and 2019 Best Paper Awards from IEICE communication society, and the 24th Telecom System Technology Award from the Telecommunication Advancement Foundation.



Daichi Shirase received the B.E. and M.E. degree in communication engineering from Osaka University, Osaka, Japan in 2020 and 2022, respectively. In 2022, he joined NEC Corporation as a researcher. His research interests include belief propagation, iterative detection, signal processing, and wireless communication.